Single-Phase Bidirectional High Frequency Link Photovoltaic Inverter with Reactive Power Compensation Function

Obed Enrique Ochoa Robles, José Antonio Beristáin Jiménez, Javier Pérez Ramírez
Dpt. of Electrical and Electronics Engineering
Sonora Institute of Technology
Obregón City, Sonora, México
E-mail: oochoa49976@alumno.itson.edu.mx, jose.beristain@itson.edu.mx, javier.perezr@itson.edu.mx

***Abstract*— This paper introduces the study of a single phase bidirectional high frequency link inverter for photovoltaic application in grid tie system, based in the Push-Pull topology. The main advantages of high frequency link inverters are: the low cost and high power density of the transformers, and the capacity to provide galvanic isolation between the photovoltaic panels and the grid. Furthermore, the capability to manage bidirectional power flow from the electric grid to the dc source allows add the capability to compensate reactive power in the system using the same circuit. Proper operation of the proposed system has been validated through simulation results, showing that the injection of photovoltaic power to the mains and reactive power compensation are carry out at the same time.**

Keywords*— *Bidirectional power flow, high frequency link; power active injection; power factor correction; power quality; power reactive compensation.

I. INTRODUCTION

Among the renewable energy resources, the photovoltaic (PV) energy is considered the most essential sustainable resource as it is available in abundance. Although this energy is intermittent in nature; however, nowadays the PV systems collect the maximum possible power absorbed by the PV panels for deliver to electric grid or feeding stand-alone loads [1]. The PV energy cost is more expensive than others generation systems of energy, for this reason the PV systems must increase its functions for maximize its use and make them feasible.

In the present time there are approaches for expand the functions of the grid-connected PV inverter, adding reactive power compensation; some of these works do not present galvanic isolation [2]-[4]; whereas in other works galvanic isolation with a low frequency transformer is included. But, the transformer is bulky and expensive because is designed for low frequency [5]. One way to reduce the transformer size is to use a high frequency isolation converter that allows to increase the power density and to reduce its cost [6]-[8]. In [9] authors suggest to work with PV array in parallel because of low voltage in the dc bus which provide more security and it extends the lifetime of the system. However, to work with low voltages involves to raise the dc voltage for injecting active power to electric grid. One of the best ways to raise the dc voltage is to use a high frequency transformer, this is due to the advantages before mentioned.

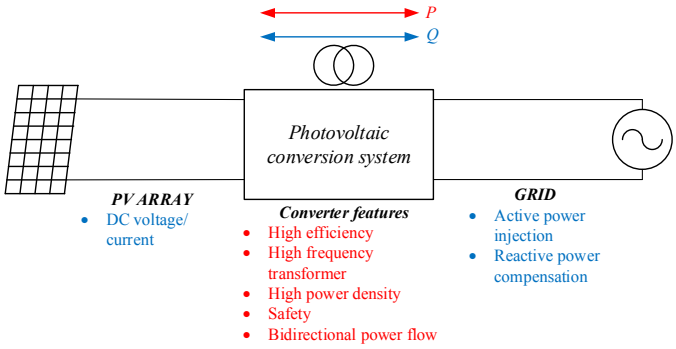

Fig. 1. Main features of the proposed system

Fig. 1 shows the proposed PV grid-connected system. The main advantages of this system are: high efficiency due to simple used topology since it contains fewer components in comparison with others topologies; galvanic isolation by high frequency transformer; electric security due to isolation between dc side and the electric grid; and finally the capability to manage bidirectional power flow, that allows injecting active power and compensating reactive power.

The approach of this paper is to use a bidirectional isolation inverter with High Frequency Link (HFL), for active power injection to electric grid, from photovoltaic cells, and to add the capability to compensate reactive power of electric grid. Where the Push-Pull topology is used, due to it has the desired features: high efficiency, high power density, safety and bidirectionality of power flow. Is important to mention that this topology has been used commonly in active power injection; in this case, it is shown how this topology is used to compensate reactive power and injection of active power to the grid, simultaneously.

This paper is organized as follows: next section presents the working of the inverter, and the obtaining of its mathematical model. In section III elements sizing of the inverter is developed. Section IV contains the modulation scheme and the control strategy. Section V shows the simulation results. Conclusions are exposed in section VI.

II. SINGLE PHASE HIGH FREQUENCY LINK INVERTER

A. The system description

The diagram of the proposed system for PV energy injection to the electric grid and reactive power compensation is shown in Fig. 2.

The system is composed by a PV panel array, a capacitive filter (C) in the dc bus, a Push-Pull converter with two transistors (Q_1 and Q_2), a high frequency transformer (HFT), a cycloconverter with four transistors (Q_3-Q_6), and an inductance (L) for the coupling with the electric grid. Also an ac load in parallel with the grid is considered.

The PV array provides active power to the Push-Pull converter via a dc bus; the capacitive filter helps to reduce the voltage ripple in the dc bus; additionally, the energy needed to compensate reactive power is stored in this element. Transistors Q_1 and Q_2 are switched in a complementary way through a high frequency square signal; it allows to convert dc voltage into a high frequency ac voltage. The resulting ac voltage is fed to the primary winding of the HFT; as a result, a high frequency isolation is achieved and the output ac voltage in the secondary winding is proportional to the transformation ratio.

The cycloconverter takes the high frequency ac voltage from the secondary winding of the HFT; using a modulation scheme, it produces an output voltage with a fundamental component at the frequency of the grid and a high frequency component at the double of the frequency used in the Push-Pull converter. An inductance L is used to couple the output voltage of the converter with the electric grid. The value of L determines the magnitude of the current ripple and the amount of reactive power that the system is capable to compensate.

B. Modeling using switching functions

To obtain the switching model of the inverter the circuit diagram in Fig. 3 is redrawn. The transistors Q_1 and Q_2 are substituted by switches S_1 and S_2, the transistors Q_3 and Q_4 are represented by the bidirectional switch S_3, and the transistors Q_5 and Q_6 by S_4. The switches S_1 and S_2 work complementarily, the same thing occurs for S_3 and S_4. The power losses of the inverter are modeled by the resistance (R).

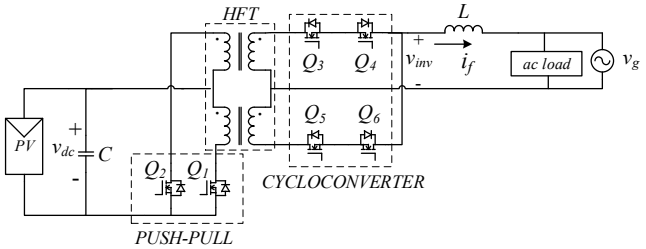

Fig. 2. Circuit diagram of the bidirectional HFL inverter

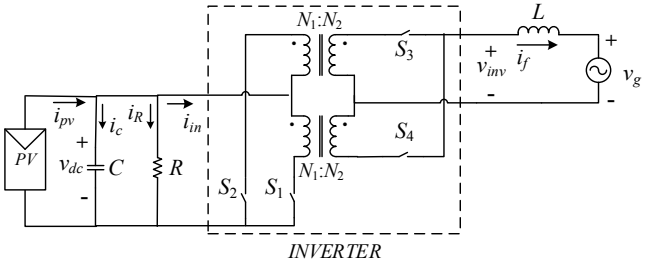

Fig. 3. Equivalent circuit diagram of the bidirectional HFL inverter using switches

To model the inverter a truth table is made using the voltages and currents that define the behavior of the inverter as shown in TABLE I. The voltage v_{dc} represents the dc bus voltage, i_{pv} the PV array dc current, i_{in} the input current of Push-Pull converter, v_{inv} the voltage of the inverter (ac bus), and i_f the ac current injected to the grid by the inverter. For simplification purposes the transformation ratio of the HFT is renamed as $\frac{N_2}{N_1} = n$.

TABLE I. TRUTH TABLE FOR SWITCHING MODEL

Commutation elements				*Currents and voltages in circuit*	
S_1	S_2	S_3	S_4	v_{inv}	i_{in}
0	1	0	1	nv_{dc}	ni_f
0	1	1	0	$-nv_{dc}$	$-ni_f$
1	0	0	1	$-nv_{dc}$	$-ni_f$
1	0	1	0	nv_{dc}	ni_f

[a] "1" if switch is closed, "0" if switch is open.

The behavior of the inverter, using the switching functions based on TABLE I. , is expressed as follows:

$$v_{inv} = n(S_1 - S_2)(S_3 - S_4)v_{dc} = nS\ v_{dc} \quad (1)$$

$$i_{in} = n(S_1 - S_2)(S_3 - S_4)i_f = nS\ i_f\ . \quad (2)$$

Equation (1) describes the output voltage of the inverter and (2) the input current. Representing (1) and (2) with its equivalent voltage and current sources, and adding the elements on Fig. 3, the switching model is shown in Fig. 4.

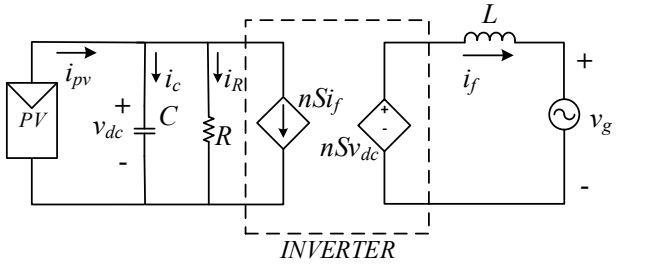

Fig. 4. Equivalent switching model of the HFL inverter

The expressions for the switching model of the complete system are given by:

$$\frac{dv_{dc}}{dt} = \frac{1}{C}\left(i_{pv} - \frac{v_{dc}}{R} - nSi_f \right) \tag{3}$$

$$\frac{di_f}{dt} = \frac{1}{L}\left(nSv_{dc} - v_g \right). \tag{4}$$

The following expression is the average operator:

$$\tilde{x}(t) = \frac{1}{T}\int_{t-T}^{t} x(\tau) d\tau \,. \tag{5}$$

The average operator in (5) is applied to (1) and (2), and the average model of the inverter is obtained [10].

$$\tilde{v}_{inv} = nu\ v_{dc} \tag{6}$$

$$\tilde{i}_{in} = nu\ i_f \ , \tag{7}$$

where *u* is the average of the switching function.

Henceforth, it will be considered the averaged values of voltages and currents in circuit, but they will not be denoted by the symbol (~) for simplicity.

Substituting the switching functions *S* in (3) and (4), for their average value *u*, the average model of the system is described by:

$$\frac{dv_{dc}}{dt} = \frac{1}{C}\left(i_{pv} - \frac{v_{dc}}{R} - nui_f \right) \tag{8}$$

$$\frac{di_f}{dt} = \frac{1}{L}\left(nuv_{dc} - v_g \right). \tag{9}$$

III. SIZING OF PASSIVE ELEMENTS

The bidirectional HFL inverter executes two tasks. First, the inverter performs the injection of active power to the grid from photovoltaic panels. Second, the inverter performs the reactive power compensation. The sizing of passive elements is carry out taking into account the power flow analysis developed in [10].

A. Coupling inductance sizing

Considering the average model of the inverter, and using a phasorial representation that is shown in Fig. 5, the sizing of coupling inductance is carried out. Inverter output voltage has a phase angle (α) with respect to electric grid and an amplitude V_m. The grid voltage is given by $v_g = V_p \cos(\omega t)$, where V_p is the magnitude and ω is the grid angular frequency of v_g.

From Fig. 5, the expression for the current I_f, is:

$$I_f = \frac{V_m \cos\alpha + jV_m \sin\alpha - V_p}{j\omega L} \tag{10}$$

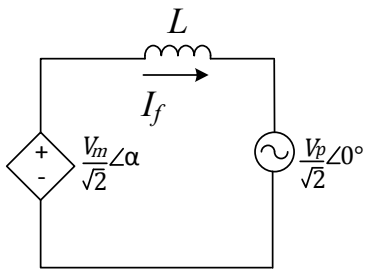

Fig. 5. Equivalent circuit for power flow analysis

From the complex power $S = VI_f^*$, active power and reactive power are given by:

$$P = \frac{V_m V_p}{2\omega L}\sin(\alpha) \tag{11}$$

$$Q = \frac{V_m V_p(\alpha)}{2\omega L}\cos(\alpha) - \frac{V_p^{\,2}}{2\omega L} \tag{12}$$

Solving for L in (11), we obtain:

$$L = \frac{V_m V_p \sin(\alpha)}{2\omega P} \tag{13}$$

where $\alpha = \arcsin\left(-\frac{PV_p}{V_m\sqrt{Q^2+P^2}} \right) - \arctan\left(\frac{-P}{Q} \right)$.

Considering absolute value or magnitude of P and Q. In this way *L* can be sizing.

B. Capacitor sizing

Fig. 6 shows the equivalent circuit for dimensioning the dc bus capacitor.

The equation that express the current of the capacitor is:

$$i_C = i_{pv} - i_R - nui_f \tag{14}$$

The equation for the capacitor voltage, is given by:

$$\frac{dv_{dc}}{dt} = \frac{1}{C}\left(i_{pv} - i_R - nui_f \right) \tag{15}$$

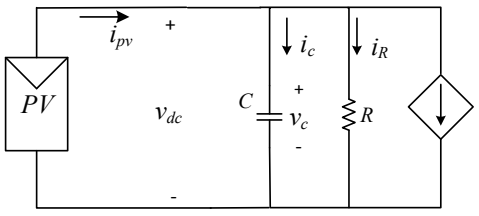

Fig. 6. Equivalent input average circuit model

Considering $u = m\cos(\omega t + \alpha)$ and $i_f = I_p \cos(\omega t + \phi)$, where m is the modulation index, I_p is the magnitude of i_f and ϕ is the phase angle with respect to v_g.

To simplify the analysis, the following approximations are made: $\alpha \approx \phi \approx 0$, converter losses are neglected and PV current is considered constant.

The expression to size the capacitor is given by:

$$C = \frac{nmI_P}{2\omega\Delta v_{dc}}, \tag{16}$$

where Δv_{dc} is a peak-to-peak dc bus voltage ripple.

For the maximum capacitive power transference modulation index must be set to one (m=1).

Considering $S = VI^* = \frac{V_P I_P \cos(\phi)}{2} - j\frac{V_P I_P \sin(\phi)}{2}$, therefore P y Q are given by:

$$P_{\max} = \frac{V_P I_P}{2}\cos(\phi) \tag{17}$$

$$Q_{\max} = \frac{V_P I_P}{2}\text{sen}(\phi) \tag{18}$$

Solving for I_P in (17) and (18), and replacing in (16).

$$C = \frac{nP_{\max}}{\omega\Delta v_{dc} V_P \cos(\phi)} \tag{19}$$

$$C = \frac{nQ_{\max}}{\omega\Delta v_{dc} V_P \sin(\phi)} \tag{20}$$

Where: $\phi = \tan^{-1}\left(\frac{Q_{\max}}{P_{\max}}\right)$

Transformation ratio (n) affects directly to capacitor size. It means that if the capacitor manages lower voltage, a higher capacitance is required in order to maintain a small ripple of voltage at the dc bus.

IV. Modulation scheme

A. Modulation strategy

To perform the sinusoidal PWM, a control signal, u, with a triangular signal are compared. In Fig. 7, the logic diagram for the activation signals of the transistors S_3 and S_4 are shown. This activation signals depend on PWM signal and activation signals of S_1 and S_2. This logic circuit is obtained from TABLE II.

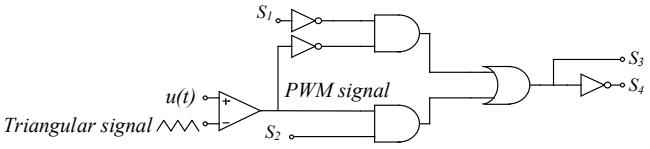

Fig. 7. Logic circuit for modulation strategy

TABLE II. Truth table for modulation strategy

Push-Pull Converter			*Modulated signal*	*Cycloconverter*		
S_1	S_2	Vs	PWM	S_3	S_4	v_{inv}
1	0	nv_{dc}	0	0	1	$-nv_{dc}$
0	1	$-nv_{dc}$	0	1	0	$-nv_{dc}$
1	0	nv_{dc}	1	1	0	nv_{dc}
0	1	$-nv_{dc}$	1	0	1	nv_{dc}

B. Control strategy

The control strategy proposed is known as a cascade control, which is used in [10]. The control scheme of the converter is shown in Fig. 8. This scheme consists of two loops, one inner loop for tracking the current (i_f) and one outer loop for regulating the voltage in dc bus (v_{dc}). Even more, the outer loop output serves as reference to the inner loop. Fig. 8 shows that the reference signal is composed by the active and reactive components of current, which are linearly independent.

V. Simulation results

To validate the converter capacity to inject, PV power to the grid and compensate reactive power, the proposed scheme was performed with parameters shown in TABLE III.

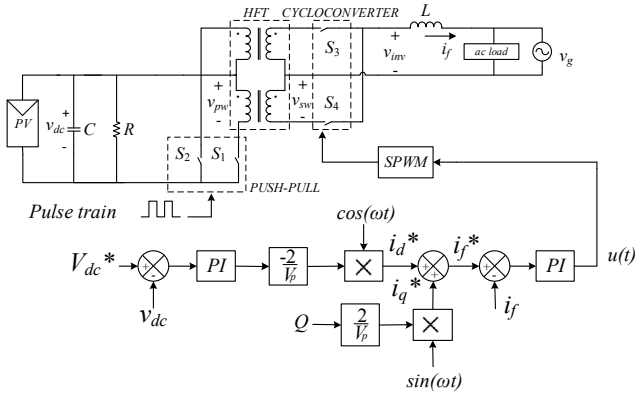

Fig. 8. Circuit diagram of the system

Four photovoltaic panels connected in parallel are considered. Each one has a maximum power point voltage of 29.8 V and a maximum power point current of 8.39 A in a Standard Test Conditions (STC). Also a 1 kvar load in parallel with the grid is considered.

TABLE III. MAIN DESIGN SPECIFICATION AND CIRCUIT PARAMETERS

Parameter	Value
v_{dc}	29.8 V
i_{pv}	33.56 A
R	9 Ω
C	62 mF
Δv_{dc}	4 V
L	3.5 mH
$f_{s\_push\text{-}pull}$	4.8 kHz
$f_{s\_cycloconverter}$	9.6 kHz
V_p	180 V
n	12
$ac\ \ load$	1 kvar
Q	1 kvar
P	1 kW
$PI_{internal\_loop}$	Gain= 0.005, tc= 0.00005
$PI_{external\_loop}$	Gain= 60, tc= 0.1

In order to show the inverter operation, waveforms of Fig. 9 are presented. In a) the ac low voltage in primary winding with a switching frequency of 4.8 kHz is presented. In b) the voltage of secondary winding which is similar to primary voltage but multiplied by the transformer turn ratio. In c) the bipolar PWM inverter output voltage has a switching frequency of 9.6 kHz. Note that transformer works at 4.8 kHz, and the cycloconverter operates at 9.6 kHz.

The proposed control scheme establishes as a voltage reference the maximum power point voltage from the PV panels, which corresponds to the maximum available power at PV array. Then, the control must adjust α and V_m of the v_{inv}, to deliver maximum power to the grid.

On the other hand, the control must adjust the amplitude of v_{inv}, for performing the reactive power compensation.

In order to test the functionality of the bidirectional HFL inverter for injecting active power and compensate reactive power, a simulation is made. Fig. 10 shows the different simulation times. In a) the dc bus voltage is shown under different conditions: from 0 s to 1 s without PV array; from 1 s to 2 s with the PV array connected; and from 2 s to 3 s carrying out active power injection and reactive power compensation, where the ripple voltage increment is observed. In b) the reactive power compensation is shown, which occurs from 2 s to 3 s. In c) the active power injection is presented, which occurs from 1 s to 2 s. And finally in d) the inductor current is shown in the different stages. Note that injection of active power and compensation of reactive power are carried out simultaneously from 2 s.

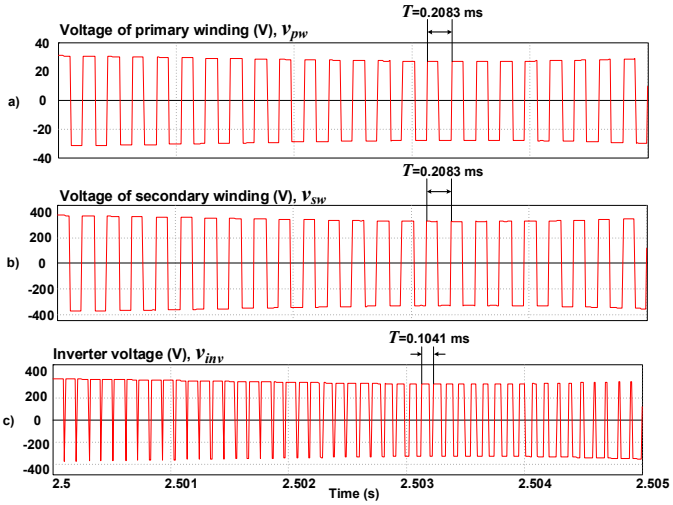

Fig. 9. Voltage waveforms of bidirectional HFL inverter. From top to bottom: a) voltage of primary winding (v_{pw}), b) voltage of secondary winding (v_{sw}) and c) inverter voltage (v_{inv})

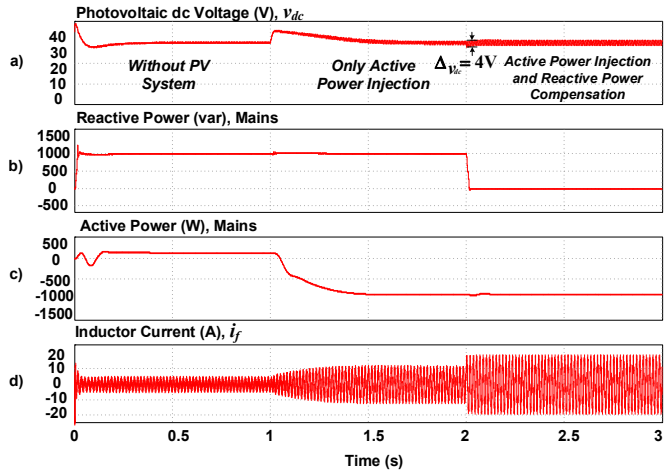

Fig. 10. Simulation results. From top to bottom: a) photovoltaic dc voltage (v_{dc}), b) reactive power (mains), c) active power (mains) and d) inductor current (i_f)

According to Fig. 10, as the inductor current increases, the voltage ripple on the capacitor increases. When PV array has a 1 kW available, 0.1 kW (10%) is used to compensate the converter losses and the 0.9 kW (90%) is injected to the electric grid. At the same time 1 kvar is compensated. This P and Q supplied to the grid generate 4 V of voltage ripple in v_{dc} as proposed in the design.

VI. CONCLUSIONS

In this paper a single-phase bidirectional HFL inverter with electric grid connection for PV systems applications was presented. The purpose of this work which is to inject active power and compensate reactive power simultaneously from PV panels was demonstrated. Moreover, the sizing of passive elements for the maximum power management was presented. The isolation with a small transformer was achieved; however, it has the committed to increase the capacitor size. Simulation

results demonstrate the capabilities of the bidirectional HFL inverter to inject active power and compensate reactive power.

REFERENCES

[1] Tharani, K.; Dahiya, R., "PV module integration with STATCOM for reactive power compensation," Computational Intelligence on Power, Energy and Controls with their impact on Humanity (CIPECH), 2014 Innovative Applications of , vol., no., pp.400,404, 28-29 Nov. 2014.

[2] Campanhol, L.B.G.; da Silva, S.A.O.; Sampaio, L.P.; Junior, A.A.O., "A grid-connected photovoltaic power system with active power injection, reactive power compensation and harmonic filtering," Power Electronics Conference (COBEP), 2013 Brazilian , vol., no., pp.642,649, 27-31 Oct. 2013.

[3] Maknouninejad, A.; Kutkut, N.; Batarseh, I.; Zhihua Qu, "Analysis and control of PV inverters operating in VAR mode at night," Innovative Smart Grid Technologies (ISGT), 2011 IEEE PES , vol., no., pp.1,5, 17-19 Jan. 2011.

[4] Hyo-Ryong Seo; Gyeong-Hun Kim; Seong-Jae Jang; Sang-Yong Kim; Sangsoo Park; Minwon Park; In-Keun Yu, "Harmonics and reactive power compensation method by grid-connected Photovoltaic generation system," Electrical Machines and Systems, 2009. ICEMS 2009. International Conference on , vol., no., pp.1,5, 15-18 Nov. 2009.

[5] Carranza Castillo, O.; Ortega Gonzalez, R.; Rodriguez Rivas, J.J., "Comparison of synchronization techniques to the grid applied to single-phase inverters," Power Electronics for Distributed Generation Systems (PEDG), 2013 4th IEEE International Symposium on , vol., no., pp.1,6, 8-11 July 2013.

[6] Young Roc Kim; Byung Hun Ra; Sung Hwon Kim; Young Hoon Son; Seok Ki Kim, "Development of 10kW grid-connected photovoltaic inverter with high frequency transformer," Electrical Machines and Systems, 2007. ICEMS. International Conference on , vol., no., pp.346,348, 8-11 Oct. 2007.

[7] Shungang Xu, "Design of photovoltaic high frequency link inverter based on push-pull forward converter," Communications, Circuits and Systems (ICCCAS), 2010 International Conference on , vol., no., pp.593,596, 28-30 July 2010.

[8] Deshang Sha; Guo Xu; Xiaozhong Liao, "Control Strategy for Input-Series-Output-Series High-Frequency AC-Link Inverters," Power Electronics, IEEE Transactions on , vol.28, no.11, pp.5283,5292, Nov. 2013.

[9] Harb, S.; Kedia, M.; Haiyu Zhang; Balog, R.S., "Microinverter and string inverter grid-connected photovoltaic system — A comprehensive study," Photovoltaic Specialists Conference (PVSC), 2013 IEEE 39th , vol., no., pp.2885,2890, 16-21 June 2013.

[10] Pérez Ramírez, J., “Multilevel converters application to static reactive power compensator STATCOM,” Doctoral Thesis, Autonomous university of San Luis Potosí, 2012. (In Spanish)

[11] Blaabjerg, Frede; Ma, Ke; Yang, Yongheng, "Power Electronics for Renewable Energy Systems ?? Status and Trends," Integrated Power Systems (CIPS), 2014 8th International Conference on , vol., no., pp.1,11, 25-27 Feb. 2014.